Supplementary Material – A localized thickened flame model for simulations of flame propagation and autoignition under elevated pressure conditions

Hiroshi Terashima[a,*], Yutaka Hanada[b], Soshi Kawai[b]

[a]*Division of Mechanical and Aerospace Engineering, Hokkaido University, N13 W8, Kita-ku, Sapporo, Hokkaido 060-8628, Japan*
[b]*Department of Aerospace Engineering, Tohoku University, 6-6-01, Aramaki-Aza-Aoba, Aoba-ku, Sendai, Miyagi 980-8579, Japan*

Details of numerical methods

Numerical schemes

This study uses the spatially-filtered compressible Navier-Stokes equations for the governing equations. An operator-splitting method [S1] is applied to solve the governing equations. The fluid and chemical reaction parts are solved separately in the temporal direction and variables are exchanged at each time step [S2]. In the fluid part, the spatially-filtered compressible Navier–Stokes equations are solved by assuming chemically frozen flows, that is, $\dot{\omega}_s = 0$ where $\dot{\omega}_s$ is the production rate of species. The chemical reaction equations, which are derived from the spatially-filtered compressible Navier–Stokes equations under constant volume and internal energy conditions, are written as follows:

$$\bar{\rho}\frac{\mathrm{d}\tilde{Y}_s}{\mathrm{d}t} = \bar{\dot{\omega}}_s, \tag{S1}$$

$$\bar{\rho}\breve{c}_v\frac{\mathrm{d}\tilde{T}}{\mathrm{d}t} = -\sum_{s=1}^{N}\tilde{e}_s\bar{\dot{\omega}}_s, \tag{S2}$$

where ρ is the density, T is the temperature, and c_v is the specific heat at constant volume for mixtures. Y_s and e_s are the mass fraction and the internal energy of species, respectively. The spatial derivative terms are neglected in the chemical reaction part. The bar $\bar{(\cdot)}$ indicates Reynolds-filtered quantities and the tilde $\tilde{(\cdot)}$ indicates Favre-filtered quantities. The breve $\breve{(\cdot)}$ denotes that the variable is calculated using Reynolds- and Favre-filtered quantities.

Conventional numerical methods for the compressible Navier–Stokes equations are applied in the fluid part. The numerical flux is evaluated by a Harten-Lax-van Leer-constant (HLLC)

*Corresponding author:
Email address: htera@eng.hokudai.ac.jp (Hiroshi Terashima)

scheme [S3]. The monotone upstream centered scheme for conservation law (MUSCL) is used to achieve high-order spatial accuracy [S4] with the minmod limiter. The viscous, heat conduction, and diffusion terms are discretized by a second-order central differencing. The time integration is conducted by the third-order total variation diminishing (TVD) Runge-Kutta scheme [S5]. In the chemical reaction part, an extended robustness-enhanced numerical algorithm [S6], called ERENA, is applied to the time integration for the chemical reaction equations.

Thermodynamic and transport models

The thermally perfect gas is assumed in this study and the CHEMKIN-II library [S7] is used to calculate the thermodynamic property. The transport property is calculated using a code package [S8]. The mixture-averaged viscosity is modeled using an empirical approximation [S9] for a low computational cost that is analogous to the thermal conductivity used in the CHEMKIN-II library [S7]. The mixture-averaged diffusion coefficient is used and the species bundling technique [S10] is applied in the case of large hydrocarbon fuels such as *n*-butane to reduce the computational cost. *n*-butane with 113 species is bundled into 19 groups with a threshold value of 0.1. The Dufour and Soret effects are neglected in this study.

Derivation of unresolved-scale components

Equation (14) in the main manuscript,

$$\langle \dot{\omega}_{s,\mathrm{urs}} \rangle = -\frac{\chi}{\chi+1} \langle \breve{\dot{\omega}}_s \rangle, \tag{S3}$$

is rewritten using the definition, $\langle f \rangle_{\mathrm{LES}} \equiv \dfrac{1}{\Delta_{\mathrm{avg}}} \displaystyle\int_{\Delta_{\mathrm{avg}}} f \mathrm{d}x$, as

$$\frac{1}{\Delta_{\mathrm{avg}}} \int_{\Delta_{\mathrm{avg}}} \dot{\omega}_{s,\mathrm{urs}} \mathrm{d}x = -\frac{\chi}{\chi+1} \frac{1}{\Delta_{\mathrm{avg}}} \int_{\Delta_{\mathrm{avg}}} \breve{\dot{\omega}}_s \mathrm{d}x, \tag{S4}$$

where an average interval Δ_{avg} may correspond to a computational cell size in LES. Differentiating Eq. (S4) in terms of x gives

$$\dot{\omega}_{s,\mathrm{urs}} = -\frac{\chi}{\chi+1} \breve{\dot{\omega}}_s - \frac{\mathrm{d}}{\mathrm{d}x} \left(\frac{\chi}{\chi+1} \right) \int_{\Delta_{\mathrm{avg}}} \breve{\dot{\omega}}_s \mathrm{d}x. \tag{S5}$$

As we assume a constant χ in a computational cell in this study, the second term in the right-hand side of Eq. (S5) may be neglected. Thus, we obtain the unresolved-scale component, $\dot{\omega}_{s,\mathrm{urs}}$, represented in Eq. (16) in the main manuscript. The same holds for the viscosity, thermal conductivity, and diffusion coefficients.

Results

Laminar flame propagation in an open space

The supplemental data for section 3.1 in the main manuscript is presented. Figure S1 shows the flame propagating speeds under 10 atm in terms of the user-specified constants, C_χ, in the case of $n = 0$ in the LTF model (Eq. (17) in the main manuscript). In contrast to the results with $n = 1$ in Fig. 1, the results with $n = 0$ show that the different grid size has a different suitable value of C_χ (e.g., for a grid size of 80 μm, $C_\chi = 30$ well predicts the DNS propagation speed, whereas $C_\chi = 100$ is needed for a grid size of 320 μm). Figure S2 shows the number of grid points in a flame region defined with Eq. (23) in the main manuscript. It is confirmed that a flame is resolved with the different number of grid points in the case of $n = 0$. An appropriate user-specified constant depends on employed grid sizes and needs to be adjusted in simulations when $n \neq 1$ is applied.

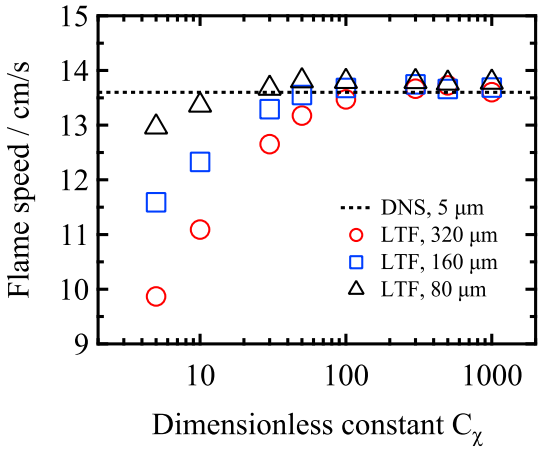

Figure S1: Flame propagation speed under 10 atm in terms of the dimensionless constant C_χ in the case of $n = 0$ in Eq. (17).

Autoignition and circular flame propagation in a two-dimensional open space

The results of autoignition and circular flame propagation in a two-dimensional (2-D) open space are presented to investigate the multi-dimensional performance of the proposed LTF model. The simulation is conducted in a 10 m $\times$ 10 m rectangular domain (-5 m $\leq x$ & $y \leq 5$ m), that is filled with a stoichiometric CH_4/air premixed mixture gas of 300 K under 1 atm. A circular-shaped hot spot of 1500 K is initially imposed on the center of the domain with the radius of 0.5 cm for inducing autoignition and flame propagation. An error function is used to smoothly connect the high-temperature region (1500 K) to the surrounding region (300 K). Uniformly

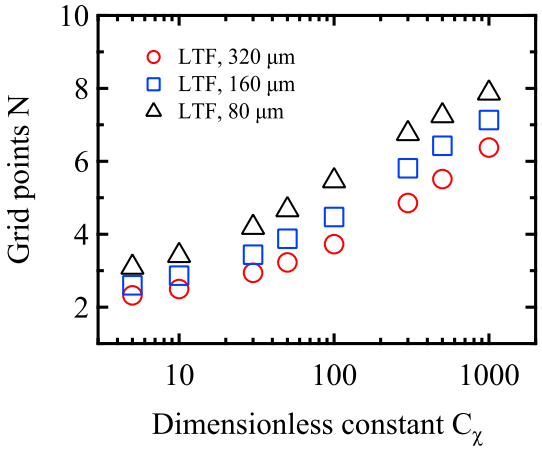

Figure S2: Number of grid points in a flame region in terms of the dimensionless constant C_χ in the case of $n = 0$ in Eq. (17).

spaced grid is used for the region of $|x| \leq 6$ cm and $|y| \leq 6$ cm, and the grid spacing is coarsened toward the boundary to minimize boundary effects. The Dirichlet condition is applied to all the boundaries. The reaction mechanism is the same as that used for the 1-D study in the main manuscript. In the LTF model, $\delta_L = 0.044$ cm, $T_{\text{ad}} = 2224$ K, and $C_\chi = 100$ are used. A reference solution (denoted as DNS solution) is obtained using the grid size of 40 μm.

Figure S3 shows the comparisons of temperature distributions at $t = 10$ ms, where the result of the LTF model is obtained with a coarse grid size of 320 μm. The result of the LTF model agrees well with that of the DNS despite the use of much coarser grid size. In contrast, no LTF model with the coarse grid size (i.e., DNS with insufficient grid resolution) induces spurious angular flame and flame instability due to the lack of grid resolution. Figure S4 compares the time history of the flame position in the radial (x) direction. Although there is a slight discrepancy between the DNS and LTF, the difference originates from the induced velocity ahead of the flame, and the flame speed obtained by the LTF agrees well with the DNS. In contrast, the flame speed is decelerated due to the spurious flame front configuration in the case of no LTF model. In conclusion, the LTF model successfully captures the autoignition and 2-D circular flame propagation behavior despite the use of coarse grid size, while not inducing spurious flame front and instability as those generated with no LTF model. This 2-D problem demonstrates the multi-dimensional capability of the proposed LTF model.

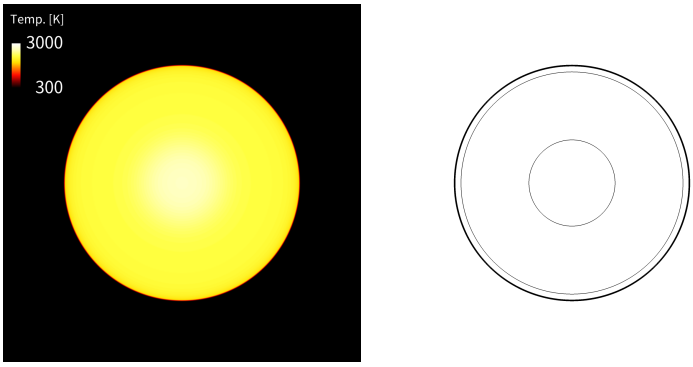

(a) DNS with 40 μm

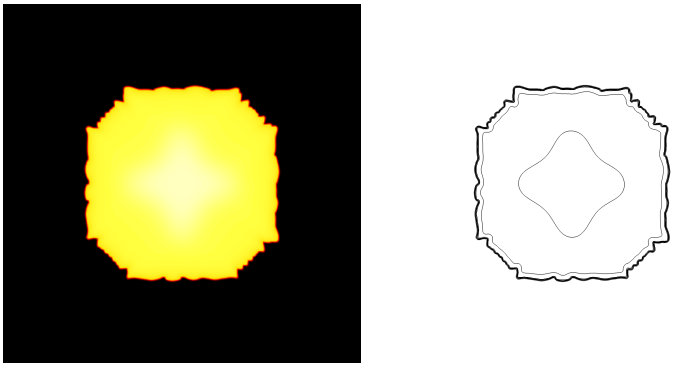

(b) No LTF with 320 μm

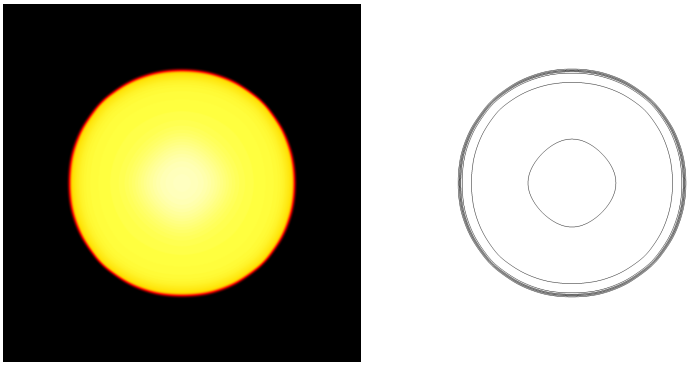

(c) LTF with 320 μm

Figure S3: Comparisons of temperature distributions at t = 10 ms. Right figures, 10 equally spaced contours from 300 to 3000 K.

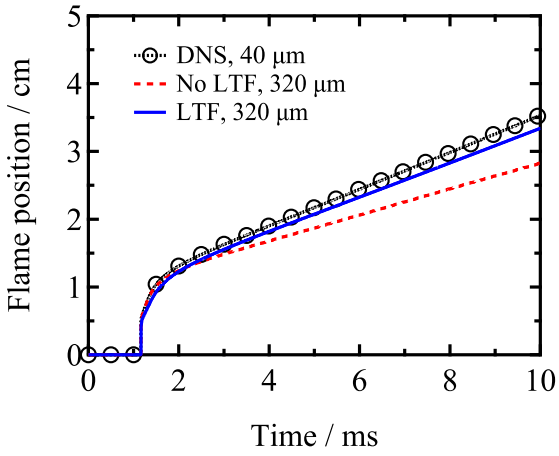

Figure S4: Comparisons of time histories of flame position in the radial (x) direction.

References

[S1] G. Strang, On the construction and comparison of difference schemes, SIAM J. Numer. Anal. 5 (1968) 506–517.

[S2] R. P. Fedkiw, B. Merriman, S. Osher, High accuracy numerical methods for thermally perfect gas flows with chemistry, J. Comput. Phys. 132 (1997) 175–190.

[S3] E. F. Toro, M. Spruce, W. Speares, Restoration of the contact surface in the HLL-Riemann solver, Shock Waves 4 (1994) 25–34.

[S4] B. Van Leer, Flux-vector splitting for the Euler equation, Springer, 1997.

[S5] S. Gottlieb, C.-W. Shu, Total variation diminishing Runge-Kutta schemes, Math. Comput. 67 (1998) 73–85.

[S6] Y. Morii, H. Terashima, M. Koshi, T. Shimizu, E. Shima, ERENA: A fast and robust jacobian-free integration method for ordinary differential equations of chemical kinetics, J. Comput. Phys. 322 (2016) 547–558.

[S7] R. Kee, F. Rupley, J. Miller, CHEMKIN-II: A fortran chemical kinetics package for the analysis of gas-phase chemical kinetics, report no, Sandia National Laboratories Report SAND89-8009 (1989).

[S8] R. J. Kee, G. Dixon-Lewis, J. Warnatz, M. E. Coltrin, J. A. Miller, A fortran computer code package for the evaluation of gas-phase multicomponent transport properties, Sandia National Laboratories Report SAND86-8246 (1986).

[S9] J. Warnatz, U. Maas, R. W. Dibble, Combustion: physical and chemical fundamentals, modeling and simulation, experiments, pollutant formation, Springer, 2006.

[S10] T. Lu, C. K. Law, Diffusion coefficient reduction through species bundling, Combust. Flame 148 (2007) 117–126.